





























## The Structure and Origin of Switchbacks: Parker Solar Probe Observations

JIA HUANG <sup>1</sup>, J. C. KASPER <sup>2,3</sup>, L. A. FISK <sup>3</sup>, DAVIN E. LARSON <sup>1</sup>, MICHAEL D. MCMANUS <sup>1</sup>,  
C. H. K. CHEN <sup>4</sup>, MIHAILO M. MARTINOVIĆ <sup>5,6</sup>, K. G. KLEIN <sup>5</sup>, LUKE THOMAS <sup>3</sup>, MINGZHE LIU <sup>6</sup>,  
BENNETT A. MARUCA <sup>7,8</sup>, LINGLING ZHAO <sup>9</sup>, YU CHEN <sup>9</sup>, QIANG HU <sup>9</sup>, LAN K. JIAN <sup>10</sup>, J. L. VERNIERO <sup>10</sup>,  
MARCO VELLI <sup>11</sup>, ROBERTO LIVI <sup>1</sup>, P. WHITTLESEY <sup>1</sup>, ALI RAHMATI <sup>1</sup>, ORLANDO ROMEO <sup>1</sup>,  
TATIANA NIEMBRO <sup>12</sup>, KRISTOFF PAULSON <sup>12</sup>, M. STEVENS <sup>12</sup>, A. W. CASE <sup>12</sup>, MARC PULUPA <sup>1</sup>,  
STUART D. BALE <sup>13,1,14,4</sup> AND J. S. HALEKAS <sup>15</sup>

<sup>1</sup>Space Sciences Laboratory, University of California, Berkeley, CA 94720, USA.

<sup>2</sup>BWX Technologies, Inc., Washington DC 20001, USA.

<sup>3</sup>Climate and Space Sciences and Engineering, University of Michigan, Ann Arbor, MI 48109, USA.

<sup>4</sup>School of Physics and Astronomy, Queen Mary University of London, London E1 4NS, UK.

<sup>5</sup>Lunar and Planetary Laboratory, University of Arizona, Tucson, AZ 85719, USA.

<sup>6</sup>LESIA, Observatoire de Paris, Université PSL, CNRS, Sorbonne Université, Université de Paris, 5 place Jules Janssen, 92195 Meudon, France.

<sup>7</sup>Department of Physics and Astronomy, University of Delaware, Newark, DE 19716, USA.

<sup>8</sup>Bartol Research Institute, University of Delaware, Newark, DE 19716.

<sup>9</sup>Department of Space Science and CSPAR, The University of Alabama in Huntsville, Huntsville, AL 35805, USA.

<sup>10</sup>Heliophysics Science Division, NASA Goddard Space Flight Center, Greenbelt, MD 20771, USA

<sup>11</sup>Department of Earth, Planetary and Space Sciences, University of California, Los Angeles CA 90095, USA

<sup>12</sup>Smithsonian Astrophysical Observatory, Cambridge, MA 02138 USA.

<sup>13</sup>Physics Department, University of California, Berkeley, CA 94720-7300, USA.

<sup>14</sup>The Blackett Laboratory, Imperial College London, London, SW7 2AZ, UK.

<sup>15</sup>Department of Physics and Astronomy, University of Iowa, Iowa City, IA 52242, USA.

### ABSTRACT

Switchbacks are rapid magnetic field reversals that last from seconds to hours. Current Parker Solar Probe (PSP) observations pose many open questions in regards to the nature of switchbacks. For example, are they stable as they propagate through the inner heliosphere, and how are they formed? In this work, we aim to investigate the structure and origin of switchbacks. In order to study the stability of switchbacks, we suppose the small scale current sheets therein may work to braid and stabilize the switchbacks. Thus, we use the partial variance of increments method to identify the small scale current sheets, and then compare their distributions in switchbacks. With more than one thousand switchbacks identified with PSP observations in seven encounters, we find many more current sheets inside than outside switchbacks, indicating that these micro-structures should work to stabilize the S-shape structures of switchbacks. Additionally, with the helium measurements, we study the variations of helium abundance ratios and alpha-proton differential speeds to trace switchbacks to their origins. We find both helium-rich and helium-poor populations in switchbacks, implying the switchbacks could originate from both closed and open magnetic field regions in the Sun. Moreover, we observe that the alpha-proton differential speeds also show complex variations as compared to the local Alfvén speed. The joint distributions of both parameters show that low helium abundance together with low differential speed is the dominant state in switchbacks. The presence of small scale current sheets in switchbacks along with the helium features are in line with the hypothesis that switchbacks could originate from the Sun via interchange reconnection process. However, other formation mechanisms are not excluded.

*Keywords:* switchback, current sheet, helium, structure, origin

## 1. INTRODUCTION

Parker Solar Probe (PSP) is the first mission to touch the Sun, and it aims to uncover the solar wind properties in the inner heliosphere (Fox et al. 2016). The PSP has completed fourteen orbits by December 2022, and its deepest perihelion reached a radial distance of about 0.062 au or 13.3 solar radii ( $R_S$ ). One of the most extraordinary observations in the near-Sun environment is the prevalent presence of switchbacks, which are defined as the rapid magnetic field reversals that last from seconds to hours (e.g. Bale et al. 2019; Kasper et al. 2019; de Wit et al. 2020; Horbury et al. 2020; Mozer et al. 2020). Many new properties of switchbacks are uncovered, which also bring new challenges to be explained.

The origin of switchbacks is a primary question to be answered, and current studies indicate the switchbacks could form either in the interplanetary space or from the Sun.

Several works support the switchbacks are formed in the interplanetary space. With the Helios observations from 0.3 au to 1 au, Macneil et al. (2020) find the total sampled time of switchbacks (durations larger than 40 seconds) increases with radial distances, implying the switchbacks could form in the interplanetary space through processes such as velocity shears, draping over ejecta, or waves and turbulence. Furthermore, Squire et al. (2020) and Mallet et al. (2021) reveal that the switchbacks could form in-situ in the expanding solar wind based on the numerical study of the low-amplitude outward-propagating Alfvénic fluctuations. In addition, Schwadron & McComas (2021) propose a method that the switchbacks could be evolved above the Alfvén point due to the so-called super-Parker spiral that formed by the magnetic field footpoints walk from the source of slow wind to faster wind. Moreover, Larosa et al. (2021) demonstrate that there are Alfvénic, fast, and slow mode signatures in switchbacks, implying the evolution of Alfvén waves and firehose-like instabilities are the two plausible generation mechanisms of switchbacks.

In contrast, many pieces of evidence suggest that the switchbacks originate from the Sun. Based on the estimations of the size and the orientations of magnetic field deflections of switchbacks observed by PSP, Horbury et al. (2020) indicate that these events could be the manifestations of coronal jets that released via near-Sun impulsive interchange reconnection processes, which occurs between open and closed magnetic field lines (Fisk & Schwadron 2001; Yamauchi et al. 2004; Fisk 2005). This is backed by previous coronal jet observations, which suggest that the jets could erupt and propagate to the PSP space and appear as switchbacks (Nisticò et al. 2010; Sterling & Moore 2020; de Pablos et al. 2022). The hypothesis that switchbacks are formed by interchange reconnection process near the Sun is supported by several other works (e.g. Fisk & Kasper 2020; Zank et al. 2020; Liang et al. 2021; Fargette et al. 2022). The reduction of switchbacks in the sub-Alfvénic solar wind, which is first reported as the PSP entered the solar corona on 28 April 2021, may also correlate with lower magnetic reconnection rates on the surface of the Sun (Kasper et al. 2021). Furthermore, Telsoni et al. (2022) report a possible direct evidence of switchback in the solar corona by using the Metis coronagraph onboard Solar Orbiter, and they suggest that this switchback is favorably produced by interchange reconnection process. In addition, the widespread kink/Alfvén waves in the corona (Tomeczyk et al. 2007; Tian et al. 2012) provides another possibility that the Alfvénic switchbacks could be highly kinked Alfvén waves that generated in the corona and survived out to PSP distances, as shown by the latest simulations on Alfvénic fluctuations (Tenerani et al. 2020; He et al. 2020; Shoda et al. 2021). Moreover, the characteristics of the cross helicity and the directions of electron heat flux in switchbacks also support the idea that the switchbacks could be local folds of magnetic field lines that originate from the corona and travel past the spacecraft (McManus et al. 2020). Besides, some works further imply the possible relationship between the patches of switchbacks and the solar supergranulation and granulation (Bale et al. 2021; Fargette et al. 2021, 2022; Shi et al. 2022).

The compositional properties of switchbacks are pivotal to trace their source regions (Kasper et al. 2007; Abbo et al. 2016; Huang et al. 2016a, 2018), but the associated works are still limited due to data calibrations during early encounters. Bale et al. (2021) find that the alpha to proton abundance ratio increases in several patches of switchbacks, and they thus propose an origin of switchbacks from above the transition region via interchange reconnection by combining other signatures. McManus et al. (2022) further find there is no consistent compositional signature difference inside the switchbacks versus outside them by analyzing 92 switchbacks identified from PSP encounters 3 and 4. However, with the alpha data available in current encounters, we may find new clues to the origins of switchbacks based on the statistical study of the switchbacks in different solar wind conditions.

The stability of switchback structures associates directly with the evolution and the origin of switchbacks. The switchbacks are "S-shape" Alfvénic structures (Kasper et al. 2019), but whether their structures are stable has not been understood. The switchbacks are not rare in previous observations by Helios at and beyond 0.3 au (Horbury et al. 2018; Woolley et al. 2020) and other spacecraft near 1 au (e.g. McComas et al. 1996; Kahler et al. 1996; Crooker et al. 2004b; Huang et al. 2017). The striking difference of PSP observations is the unexpected prevalence of switchbacks in the near-Sun environment Kasper et al. (2019), which implies that many switchbacks should disappear from PSP space to beyond. In regard to this fact, there are several questions need to be answered. If the switchbacks originate from the Sun, then we need to explain how they could propagate to the PSP space but disappear when travel farther. If the switchbacks are formed locally, we need to know the reason why they are formed locally and why they are more prevalent in the inner heliosphere. In general, the folded magnetic field structures will stretch to radial as the solar wind propagates in the interplanetary space, thus there must be some mechanisms to help avoid the relaxations of the S-shape structures of switchbacks. Rasca et al. (2021) predict the switchbacks may survive until around 60  $R_S$  based on the evolutions of the magnetic field and speed changes in the boundaries of switchbacks. Some studies indicate that current sheets exist in the switchback boundaries (Krasnoselskikh et al. 2020; Farrell et al. 2020; Martinović et al. 2021), which implies the presence of strong electric fields in the layers to keep the system quasi-stable. These results imply that the boundaries of switchbacks may play a role to prevent the switchbacks from being destroyed. Consequently, it is valuable to investigate the structures of switchbacks to understand their stability.

In this work, we will focus on the structures and alpha particle variations in switchbacks. Following the method of Kasper et al. (2019), we identify thousands of switchbacks with PSP observations during encounters 1-8 (E1-E8)<sup>1</sup>. Based on the analysis of the current sheet distributions and alpha particle characteristics, we investigate the structure and origin of the switchbacks. The data are described in Section 2. Section 3 includes the method to identify switchbacks, the distributions of small scale current sheets and also the alpha signatures of switchbacks in E4-E8. We present the discussion and summary in Section 4 and Section 5, respectively.

## 2. DATA

The Solar Wind Electrons, Alphas, and Protons (SWEAP) instrument suite (Kasper et al. 2016) and the FIELDS instrument suite (Bale et al. 2016) onboard PSP provide the data used in this work. SWEAP includes the Solar Probe Cup (SPC) (Case et al. 2020), Solar Probe Analyzer for Electrons (SPAN-E) (Whittlesey et al. 2020), and Solar Probe Analyzer for Ions (SPAN-I) (Livi et al. 2022). SWEAP is designed to measure the velocity distributions of solar wind electrons, protons, and alpha particles (Kasper et al. 2016). FIELDS is designed to measure DC and fluctuation magnetic and electric fields, plasma wave spectra and polarization properties, the spacecraft floating potential, and solar radio emissions (Bale et al. 2016).

In this work, we use the magnetic field data from E1 to E8 to study the distributions of small scale current sheets in switchbacks, and we use the fitted proton and alpha data from SPAN-I that are available since E4 to investigate the alpha characteristics in switchbacks. SPAN-I measures three-dimensional velocity distribution functions of the ambient ion populations in the energy range from several eV/q to 20 keV/q at a maximum cadence of 0.437 s, and it has a time of flight section that enables it to differentiate the ion species (Kasper et al. 2016). The details of the fitted proton and alpha data are described in Finley et al. (2020), Livi et al. (2022) and McManus et al. (2022). However, the SPAN-I measurements used here are from low cadence downlinked data, and the time resolution of the fitted proton and alpha data are 6.99 s and 13.98 s, respectively (Finley et al. 2020; Verniero et al. 2020). The FIELDS instrument collects high resolution vector magnetic fields with variable time resolutions. The 4 samples per cycle (i.e. 4 samples per 0.874 s) data are used here.

## 3. RESULTS

### 3.1. Switchback identification

Following the method of Kasper et al. (2019), we separate a switchback into five parts: leading/trailing quiet period (LQP/TQP), leading/trailing transition region (LTR/TTR), and spike (i.e. the core structure of switchback). Figure 1 shows an example of the switchback observed on 27 April 2021 during E8. Panel (a) presents the pitch angle distributions (PADs) of suprathermal electron at energy of 316.4 eV. Panel (b) displays the magnetic field components in RTN coordinates, and panel (c) indicates the variations of the radial magnetic field component ( $B_R$ ) to the total

<sup>1</sup> E3 is excluded due to data gaps.

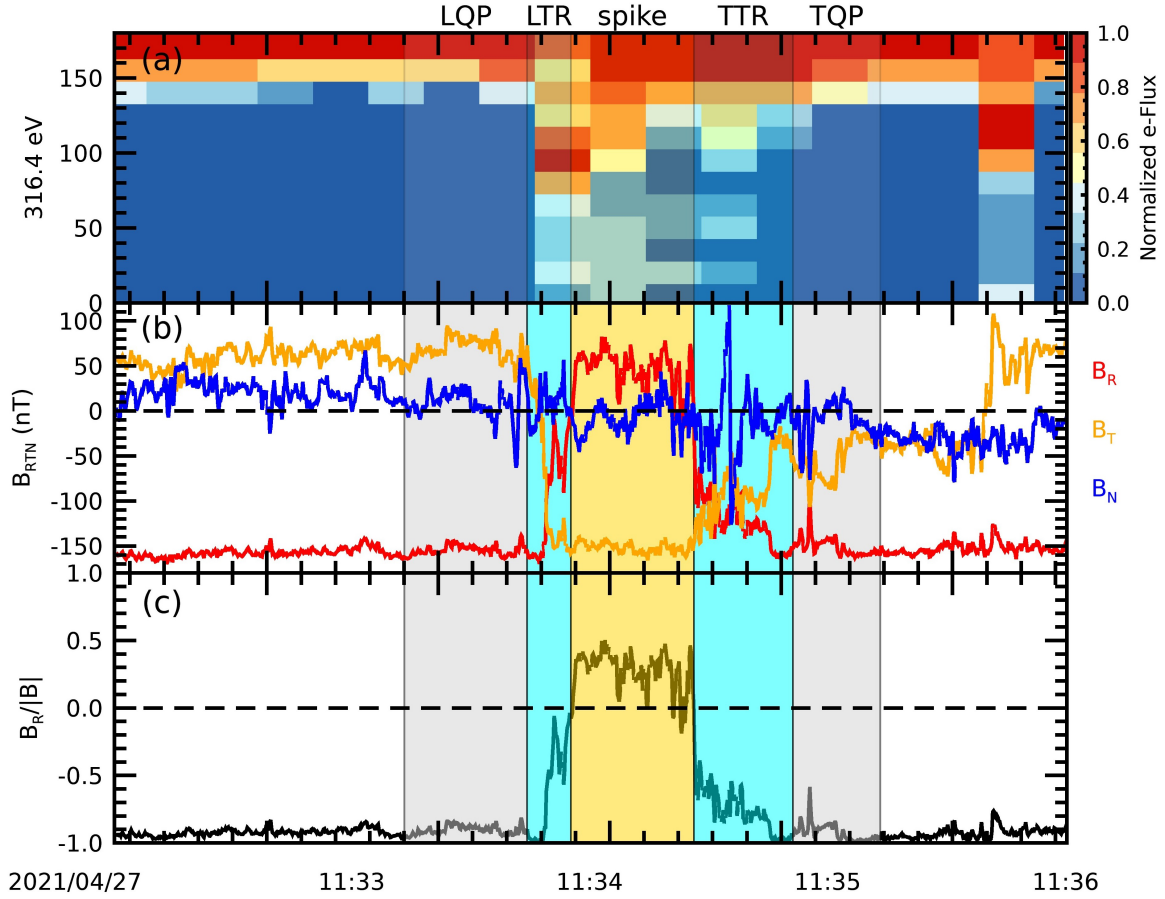


**Figure 1.** An example of switchback. From top to bottom, the panels show the normalized pitch angle distributions of suprathermal electrons at energy of 316.4 eV, the magnetic field components in RTN coordinates, and the radial to total magnetic field ratio, respectively. From left to right, the five shaded regions mark leading quiet period (LQP), leading transition region (LTR), spike, trailing transition region (TTR), and trailing quiet period (TQP), respectively.

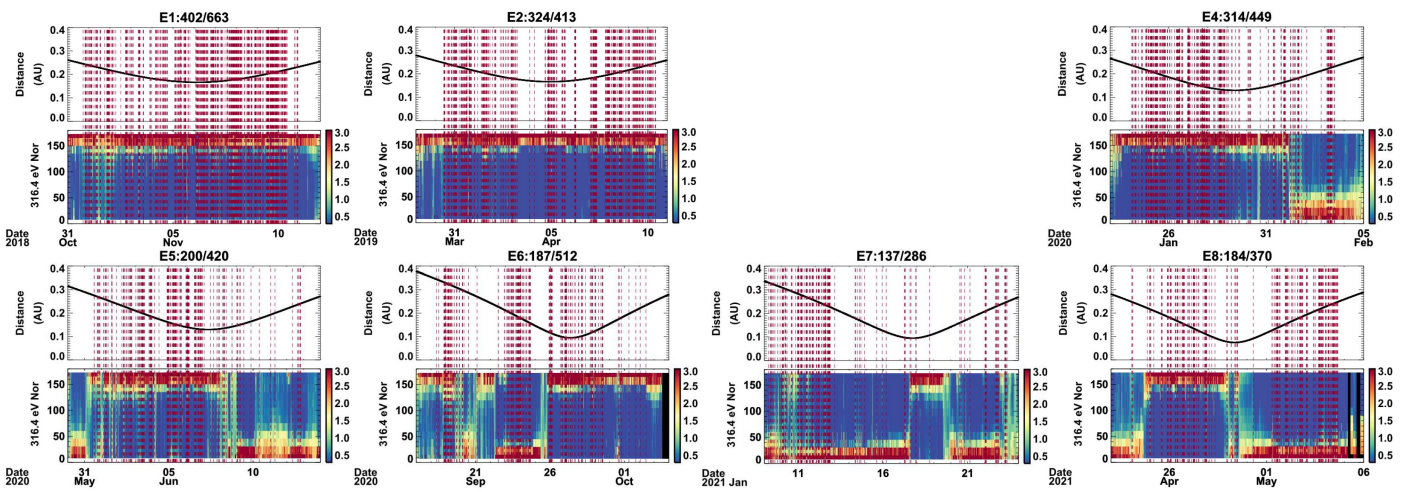


**Figure 2.** Overview of the switchbacks identified in each encounter. In each figure, the top panel shows the distance of the spacecraft to the Sun, and the bottom panel shows the pitch angle distributions of suprathermal electrons. The vertical dashed lines mark the middle time of the spike region of the switchbacks in each encounter.



magnetic field strength ( $|B|$ ), i.e.  $B_R/|B|$ . The spike is generally characterized by a fully magnetic field reversal, as shown by the yellow shaded region, where the  $B_R/|B|$  changes polarity while the dominant electron PADs keep the same. The two cyan shaded regions represent the transition regions, and they indicate the magnetic field rotates from the quiet period to the spike and usually contain large-amplitude fluctuations. The LTR (TTR) locates between the spike and the LQP (TQP), which is the steady ambient solar wind as indicated by the grey shaded regions.

We use a two-step method to identify the switchbacks in each encounter. In the first step, we develop an automatic algorithm to search the candidates of switchbacks in about 11 days around the perihelion. The searching interval is adjusted to be consistent with the time period when the SWEAP provides high time resolution plasma observations. At the beginning, we need to find the heliospheric current sheet crossings, which marks the boundaries of sectors that have different polarities (Crooker et al. 2004a; Szabo et al. 2020; Lavraud et al. 2020). Then, we search the candidates of switchbacks in the sectors that have the same polarity. In order to find prominent reversals and also as many candidates as we can, we require the  $B_R/|B|$  changes significantly from the quiet solar wind to the spike: (1) when the polarity of the sector is negative, we require  $B_R/|B| > -0.25$  in the spike and  $B_R/|B| < -0.85$  in the quiet period; (2) when the sector polarity is positive, we need  $B_R/|B| < 0.25$  in the spike and  $B_R/|B| > 0.85$  in the quiet period. We further demand there are at least three data points in the spike region. In the second step, we manually select the better switchbacks from the candidates. In this part, we use two criteria to select the better ones. On one hand, we require the electron PADs do not change their main distributions, which can help to verify the reversal of magnetic field lines is real rather than current sheets. On the other hand, we also compare the magnetic field components with the velocity components to find relatively high Alfvénic switchbacks. Consequently, we generate the lists of switchbacks for each encounter. We note that the switchbacks we identified in E1 and E2 have been used in studies by Martinović et al. (2021) and Akhavan-Tafti et al. (2021), and our switchback lists from E1 to E8 have supported the work by Akhavan-Tafti et al. (2022).

As a result, Figure 2 shows an overview of the switchbacks in each encounter. For the seven encounters, we find 663 switchback candidates in E1, 413 in E2, 449 in E4, 420 in E5, 512 in E6, 286 in E7 and 370 in E8. Among them, the good events selected for study are 402 in E1, 324 in E2, 314 in E4, 200 in E5, 187 in E6, 137 in E7, and 184 in E8. This means 1748 out of 3113 candidates are good switchbacks that suit for further study. From this figure, we can also see the signature that the switchbacks distribute as patches (Horbury et al. 2020; Woolley et al. 2020). We also note that the switchbacks are profoundly reduced near the heliospheric current sheet crossings in E4 to E8, one reason is that the multiple current sheet crossings (Szabo et al. 2020) make it harder to identify the switchbacks.

### 3.2. Current sheets in switchbacks

There are different methods to find current sheets in solar wind, here we use the partial variance of increments (PVI) method, which is a reliable tool to identify such structures (e.g. Greco et al. 2008; Podesta 2017; Greco et al. 2018; Chhiber et al. 2020; Qudsi et al. 2020). The PVI at time  $s$  is defined as the magnitude of the change in the magnetic field vector  $\mathbf{B}$  over a time lag  $\tau$ , thus

$$\text{PVI}_{s,\tau} = \frac{|\Delta\mathbf{B}(s,\tau)|}{\sqrt{\langle|\Delta\mathbf{B}(s,\tau)|^2\rangle}}, \quad (1)$$

where  $\Delta\mathbf{B}(s,\tau) = \mathbf{B}(s+\tau) - \mathbf{B}(s)$  is the increment.  $\langle\dots\rangle$  represents an average over a suitable time period. In this work, we follow Qudsi et al. (2020) to set the time lag  $\tau$  and the average interval as 0.874 s and 8 hours (several times of the correlation time (Chen et al. 2020)), respectively.

According to previous studies,  $\text{PVI} > 3$  indicates non-Gaussian structures,  $\text{PVI} > 6$  means current sheets, and  $\text{PVI} > 8$  suggests reconnection sites (Greco et al. 2018; Chhiber et al. 2020, and references therein). Therefore, we choose PVI values that larger than 6 to identify current sheets. Due to the high time resolution of magnetic field data and the cross trajectory of spacecraft, several adjacent data points with  $\text{PVI} > 6$  could belong to the same current sheet. We can either use the data points or the cases of current sheets to study the distributions. Here, we identify a current sheet case if the data point with  $\text{PVI} > 6$  is the maximum value in about 10 s, and the criterion is set due to only about 1.7% of the selected switchbacks have a waiting time shorter than 10 s. We also find the results are similar between the two methods, here we only present the distributions of the cases of current sheets in the switchbacks. For the seven encounters, the corresponding current sheet cases therein are 2461, 2438, 2541, 2834, 3388, 3670, and 3038, respectively.

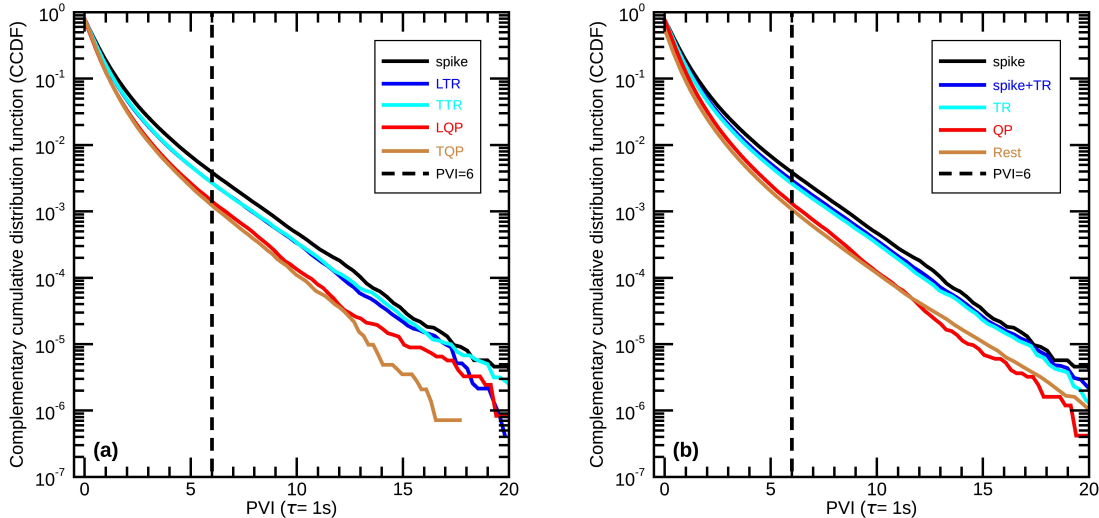


**Figure 3.** The complementary cumulative distribution function (CCDF) of PVI values in different parts of switchbacks. In panel (a), spike, leading transition region (LTR), trailing transition region (TTR), leading quiet period (LQP), and trailing quiet period (TQP) are represented by black, blue, cyan, red and brown colors, respectively. In panel (b), spike, combined region of spike and transition regions (spike+TR), combined LTR and TTR (TR), combined LQP and TQP (QP), and rest solar wind are represented by black, blue, cyan, red and brown colors, respectively. The vertical dashed lines in both panels mark the PVI value equals to 6. The switchbacks are from encounters E1-E8.

Figure 3 shows the complementary cumulative distribution function (CCDF, i.e. the probability of a variable that above a threshold) of the PVI values in different parts of switchbacks. Panel (a) shows the CCDF of PVI values in the five parts of switchbacks (spike, LTR/TTR, LQP/TQP), representing by the different color lines as shown by the legend. Panel (b) exhibits the CCDF in combined regions of switchbacks by ignoring the asymmetries in leading and trailing edges, and we also include the rest solar wind outside switchbacks ('Rest' in the figure) in the 11 days during each encounter for a comparison. TR means the combined LTR and TTR, and QP means the combined LQP and TQP. A similar figure to indicate the PVI variations in E1 and E2 is included in [Martinović et al. \(2021\)](#). Panel (a) denotes that large PVI values are more prevalent in spike (black line) and transition regions (blue and cyan lines) than that in quiet periods (red and brown lines), which is reasonable because the magnetic field generally changes smoothly in quiet periods. Moreover, it seems the leading and trailing locations of both quiet periods and transition regions do not produce large asymmetric distributions of current sheets ( $PVI > 6$ ). Panel (b) shows that the rest solar wind (brown line) has comparable current sheets with QP (red line). In addition, the spike (black line) has more current sheet densities than TR (cyan line), but the current sheet densities in the regions that include major magnetic field rotations (spike+TR, blue line) are much closer to the TR. This is a result of the longer duration but lower current sheet densities of TR, which may imply the transition regions play an important role in maintaining the structures of switchbacks. Overall, the distributions of current sheets in combined regions are consistent with the results present in panel (a).

Table 1 lists the distributions of current sheets in different regions of switchbacks in different encounters. During each encounter, the numbers of current sheets ( $N_{cs}$ ) are displayed in the first row. We then normalize the duration of each part of switchbacks to the total duration of spikes to get their relative durations ( $D_{spike}$ ), and calculate the density of current sheets ( $\rho_{cs}$ ), which is defined as the ratio of the case number to the relative duration ( $\rho_{cs} = N_{cs}/D_{spike}$ ). The relative densities in each encounter are further described as percentages ( $R$ ) in comparison with the current sheet density in spike for better visualization, whereas the  $\hat{R}$  represents the relative current sheet density normalized by that in the spike of E1 for further comparison among different encounters. The results in all encounters are shown in the bottom of the table. This table reveals several features:

1. The current sheets are most prevalent in spikes. During each encounter, we can see the density  $R$  is largest in spike and smallest in quiet periods, whereas the transition regions have the intermediate density. This is

- consistent with the results shown in Figure 3. In all encounters,  $R$  is 65.9% in TR and 33.1% in QP as compared with that in the spike.
2. The current sheet distributions in leading and trailing boundaries show slight asymmetry. In each encounter, we can see the current sheet densities in either quiet period or transition region are similar in leading and trailing edges, but  $R$  is slightly different in both sides. For all encounters, the  $R$  are 35.2% versus 29.7% in LQP and TQP, whereas 62.1% versus 69.9% in LTR and TTR, respectively. Besides, the LTR has larger  $R$  than TTR during E1 and E2, but the circumstance reverses in later encounters except E6, when the LTR and TTR have nearly the same  $R$ . The perihelia of E1 and E2 are  $\sim 0.17$  au, while the perihelia are much closer to the Sun in later encounters. The likely systematic changes imply the transition regions may evolve with radial distances from the Sun, which still needs future observations.
  3. The current sheet densities vary in different encounters. Focusing on the normalized current sheet densities  $\hat{R}$ , we can see the current sheet densities change significantly in different encounters. The  $\hat{R}$  in spike are above 1 in E2-E5 but below 1 in E6-E8, while the transition regions show much more variable  $\hat{R}$  in different encounters. However, in comparison with spike and transition regions, the quiet periods and rest solar wind have least intensive current sheets but more uniform distributions between different encounters. As the PSP dives deeper towards the Sun, the current sheet densities increase remarkably in both quiet periods and rest solar wind, implying the switchbacks may stay in a more pristine state when closer the Sun.
  4. The density in spike+TR region is determined by the TR. From the bottom of this table, we can see the current sheet density  $R$  in TR is 65.9% of that in spike, resulting in 75.7% level in spike+TR. This is a natural mathematical consequence of the longer duration but lower  $R$  in TR. But this result implies the transition regions may play a more important role in maintaining the structure of switchbacks than spike.
  5. The rest solar wind has slightly larger current sheet densities than that in the quiet periods. The QP and rest solar wind have comparable current sheets densities, which is reasonable that the QP solar wind is much close to the ambient solar wind. Specifically, the rest solar wind has higher  $R$  than QP in all encounters except E4. Additionally, the current sheet densities in both QP and rest solar wind show a general decrease trend with distance from the Sun, but the current sheets in QP seem to vanish rapider than that in the rest solar wind. The results suggest that switchback structure may dissipate start from the QP as they propagate outward.

Table 1. The distributions of current sheets in different regions of switchbacks.

	spike	LQP	LTR	TTR	TQP	spike+TR	TR	QP	Rest
E1	$N_{cs}$	24	355	241	70	939	575	94	1239
	$D_{spike}$	0.437	1.508	1.101	0.878	3.414	2.500	1.264	9.969
	$\rho_{cs}$	54.920	235.411	218.892	79.727	275.044	230.000	74.367	124.285
	$R$	<b>0.146</b>	<b>0.628</b>	<b>0.584</b>	<b>0.213</b>	<b>0.733</b>	<b>0.613</b>	<b>0.198</b>	<b>0.331</b>
	$\hat{R}$	<b>0.146</b>	<b>0.628</b>	<b>0.584</b>	<b>0.213</b>	<b>0.733</b>	<b>0.613</b>	<b>0.198</b>	<b>0.331</b>
E2	$N_{cs}$	29	223	147	51	733	362	74	1468
	$D_{spike}$	0.351	1.100	0.836	0.661	2.861	1.912	0.936	12.780
	$\rho_{cs}$	82.513	202.761	175.882	77.190	256.179	189.303	79.026	114.865
	$R$	<b>0.211</b>	<b>0.519</b>	<b>0.450</b>	<b>0.197</b>	<b>0.655</b>	<b>0.484</b>	<b>0.202</b>	<b>0.294</b>
	$\hat{R}$	<b>0.232</b>	<b>0.569</b>	<b>0.493</b>	<b>0.216</b>	<b>0.719</b>	<b>0.531</b>	<b>0.222</b>	<b>0.322</b>
E4	$N_{cs}$	79	225	318	72	742	530	144	1486
	$D_{spike}$	0.857	1.489	1.503	0.862	3.841	2.910	1.674	20.467
	$\rho_{cs}$	92.223	151.083	211.636	83.536	193.202	182.142	86.013	72.606
	$R$	<b>0.406</b>	<b>0.666</b>	<b>0.932</b>	<b>0.368</b>	<b>0.851</b>	<b>0.802</b>	<b>0.379</b>	<b>0.320</b>
	$\hat{R}$	<b>0.430</b>	<b>0.704</b>	<b>0.986</b>	<b>0.389</b>	<b>0.900</b>	<b>0.849</b>	<b>0.401</b>	<b>0.338</b>
E5	$N_{cs}$	77	234	330	74	748	529	147	1862
	$D_{spike}$	1.047	1.839	1.943	1.028	4.388	3.583	2.000	23.116
	$\rho_{cs}$	73.563	127.235	169.831	71.965	170.469	147.647	73.502	80.551
	$R$	<b>0.264</b>	<b>0.456</b>	<b>0.609</b>	<b>0.258</b>	<b>0.611</b>	<b>0.529</b>	<b>0.263</b>	<b>0.289</b>
	$\hat{R}$	<b>0.328</b>	<b>0.567</b>	<b>0.757</b>	<b>0.321</b>	<b>0.760</b>	<b>0.658</b>	<b>0.328</b>	<b>0.359</b>
E6	$N_{cs}$	143	319	325	91	864	605	225	2276
	$D_{spike}$	0.851	1.347	1.387	0.797	3.370	2.540	1.504	14.313
	$\rho_{cs}$	168.112	236.742	234.281	114.154	256.356	238.175	149.634	159.017
	$R$	<b>0.539</b>	<b>0.759</b>	<b>0.751</b>	<b>0.366</b>	<b>0.822</b>	<b>0.763</b>	<b>0.480</b>	<b>0.510</b>
	$\hat{R}$	<b>0.420</b>	<b>0.592</b>	<b>0.586</b>	<b>0.285</b>	<b>0.641</b>	<b>0.595</b>	<b>0.374</b>	<b>0.397</b>
E7	$N_{cs}$	95	288	384	104	972	632	196	2499
	$D_{spike}$	0.802	1.217	1.346	0.840	3.205	2.402	1.511	14.361
	$\rho_{cs}$	118.391	236.578	285.198	123.802	303.282	263.106	129.677	174.016
	$R$	<b>0.308</b>	<b>0.616</b>	<b>0.743</b>	<b>0.322</b>	<b>0.790</b>	<b>0.685</b>	<b>0.338</b>	<b>0.453</b>

Table 1 continued on next page

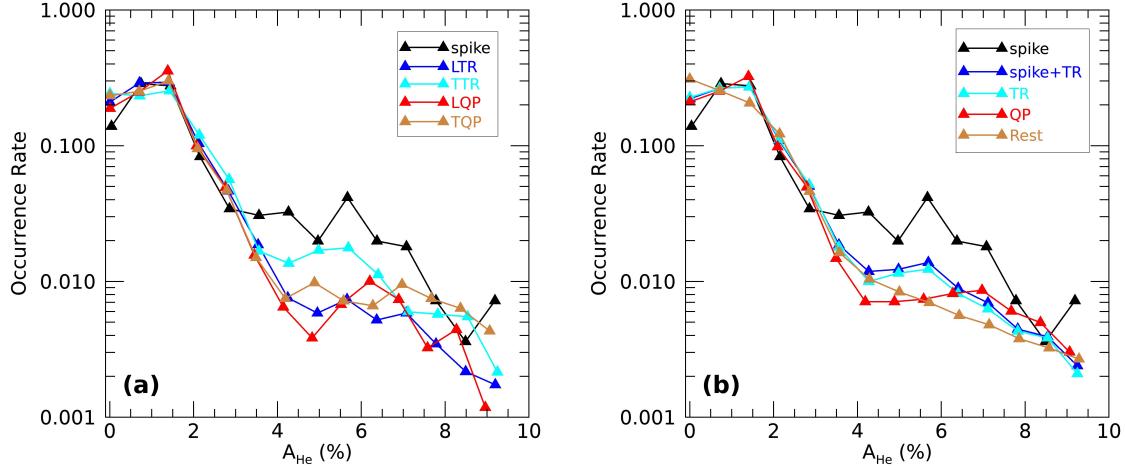


Table 1 (continued)

	spike	LQP	LTR	TTR	TQP	spike+TR	TR	QP	Rest
	$\hat{R}$	<b>0.297</b>	<b>0.594</b>	<b>0.716</b>	<b>0.311</b>	<b>0.761</b>	<b>0.660</b>	<b>0.325</b>	<b>0.436</b>
E8	$N_{cs}$	122	252	282	95	735	470	198	2074
	$D_{spike}$	0.741	1.070	1.056	0.744	2.629	1.888	1.329	11.314
	$\rho_{cs}$	164.567	235.548	267.057	127.696	279.521	248.901	148.983	183.316
	$R$	<b>1.000</b>	<b>0.496</b>	<b>0.804</b>	<b>0.385</b>	<b>0.842</b>	<b>0.750</b>	<b>0.449</b>	<b>0.552</b>
	$\hat{R}$	<b>0.870</b>	<b>0.432</b>	<b>0.700</b>	<b>0.335</b>	<b>0.733</b>	<b>0.653</b>	<b>0.391</b>	<b>0.481</b>
All	$N_{cs}$	569	1896	2027	557	5733	3703	1078	12904
	$D_{spike}$	0.702	1.328	1.261	0.816	3.292	2.443	1.415	14.311
	$\rho_{cs}$	810.235	1427.430	1607.760	682.654	1741.610	1516.050	761.643	901.718
	$R$	<b>1.000</b>	<b>0.352</b>	<b>0.699</b>	<b>0.297</b>	<b>0.757</b>	<b>0.659</b>	<b>0.331</b>	<b>0.392</b>
	$\hat{R}$	<b>0.979</b>	<b>0.345</b>	<b>0.684</b>	<b>0.290</b>	<b>0.741</b>	<b>0.645</b>	<b>0.324</b>	<b>0.384</b>

<sup>a</sup>  $N_{cs}$  means the number of current sheets in each region of switchbacks.  $D_{spike}$  is the relative duration of each region to the spike duration, and the spike duration is set to be 1 in each encounter with the actual cumulative duration listed.  $\rho_{cs} = N_{cs}/D_{spike}$  indicates the density of current sheets in each region of switchbacks.  $R$  is the ratio of the current sheet density in each region to that in the spike in each encounter.  $\hat{R}$  represents the relative current sheet density normalized by that in the spike of E1.

<sup>b</sup> Spike: complete reversal of magnetic field polarity. LQP/TQP/QP: Leading/Trailing/Combined Quiet Period. LTR/TTR/TR: Leading/Trailing/Combined Transition Region. Rest: rest solar wind, which is the solar wind between the first and the last switchback by removing all switchbacks therein during each encounter. The current sheet number  $N_{cs}$  in QP (TR) is generally smaller than the summed number in LQP and TQP (LTR and TTR) is caused by the overlap of some switchbacks.



**Figure 4.** The occurrence rates of alpha to proton abundance ratio ( $A_{He}$ ) inside and outside switchbacks. Panel (a) shows the  $A_{He}$  variations in different parts of switchbacks, and panel (b) compares their distributions in combined regions of switchbacks. Different regions of switchbacks are represented by different colors of lines, and the colors in panel (a) and panel (b) are the same to that in figure 3, respectively.

### 3.3. Helium signatures

The helium measurements give clues to the solar wind origins (e.g. Bochsler 2007; Aellig et al. 2001; Kasper et al. 2012; Huang et al. 2016b; Fu et al. 2018). The helium abundance ratio ( $A_{He} = N_{\alpha}/N_p \times 100$ ) usually is enhanced in fast solar wind and magnetic clouds, implying the helium-rich population originates from open magnetic field regions in the Sun (Borrini et al. 1981; Gosling et al. 1981; Suess et al. 2009). Nevertheless, the  $A_{He}$  in slow solar wind greatly correlates with solar activity, indicating that slow wind with decreased  $A_{He}$  (helium-poor population) at solar minimum should come from helmet streamer whereas slow wind with increased  $A_{He}$  at solar maximum mainly comes from active regions (Kasper et al. 2007, 2012; Alterman et al. 2018; Alterman & Kasper 2019).

Moreover, alpha-proton differential speed ( $V_{\alpha p}$ ) is large in fast wind and comparable to local Alfvén speed ( $V_A$ ), but  $V_{\alpha p}$  is close to zero in slow solar wind (Marsch et al. 1982; Steinberg et al. 1996; Reisenfeld et al. 2001; Berger et al. 2011). Current studies indicate bimodal distributions of  $A_{He}$  versus  $V_{\alpha p}/V_A$  in the solar wind, with high  $A_{He}$  and high  $V_{\alpha p}/V_A$  population escaping directly along open magnetic field lines as described by wave-turbulence driven models, while low  $A_{He}$  and low  $V_{\alpha p}/V_A$  population releasing through magnetic reconnection processes (Ďurovcová et al. 2017, 2019; Fu et al. 2018, and references therein). Therefore, the characteristics of  $A_{He}$  and  $V_{\alpha p}/V_A$  in switchbacks could infer their possible origins.

Following Reisenfeld et al. (2001) and Fu et al. (2018), we define the  $V_{\alpha p}$  as the field-aligned differential speed, i.e.  $V_{\alpha p} = (v_{\alpha r} - v_{pr})/\cos(\theta)$ , where  $v_{\alpha r}$  and  $v_{pr}$  are the radial speeds of alpha particle and proton, respectively, and  $\theta$  measures the angle of the magnetic field vector from radial direction. Here, we further require  $\cos(\theta) = |Br/B|$  to assure the derived differential speed is independent with magnetic field polarity, where  $Br$  and  $B$  represent the radial component and the total strength of the magnetic field, respectively. Moreover, the local Alfvén speed is calculated with  $V_A = |B|/\sqrt{\mu_0(N_p m_p + N_{\alpha} m_{\alpha})}$ , where  $\mu_0$  denotes the vacuum magnetic permeability,  $N_p$  ( $N_{\alpha}$ ) and  $m_p$  ( $m_{\alpha}$ ) are the number density and mass of proton (alpha particle), respectively. In the calculations, we use the electron density derived from the analysis of plasma quasi-thermal noise (QTN) spectrum measured by the FIELDS Radio Frequency Spectrometer (Pulupa et al. 2017; Moncuquet et al. 2020) to replace  $N_p$  by assuming charge neutrality and  $A_{He}$  is 4%, which does not significantly change the  $V_A$  as  $A_{He}$  generally varies from 1% to 8% (Liu et al. 2021; Mostafavi et al. 2022).

The fitted helium data are available since E4 and have a good quality due to the solar wind flows predominantly into the field of view of SPAN-I, thus we choose the alpha data from E4 to E8 for this part of work. The data quality is further verified by comparing the proton and alpha densities from SPAN-I with the QTN electron density. Figure 4 presents the  $A_{He}$  variations inside and outside switchbacks. Figure 4(a) denotes the occurrence rates of  $A_{He}$  in the five regions of switchbacks, marked by the colors as shown in the legend. It shows that both helium-poor ( $A_{He} \sim 1.0\%$ )

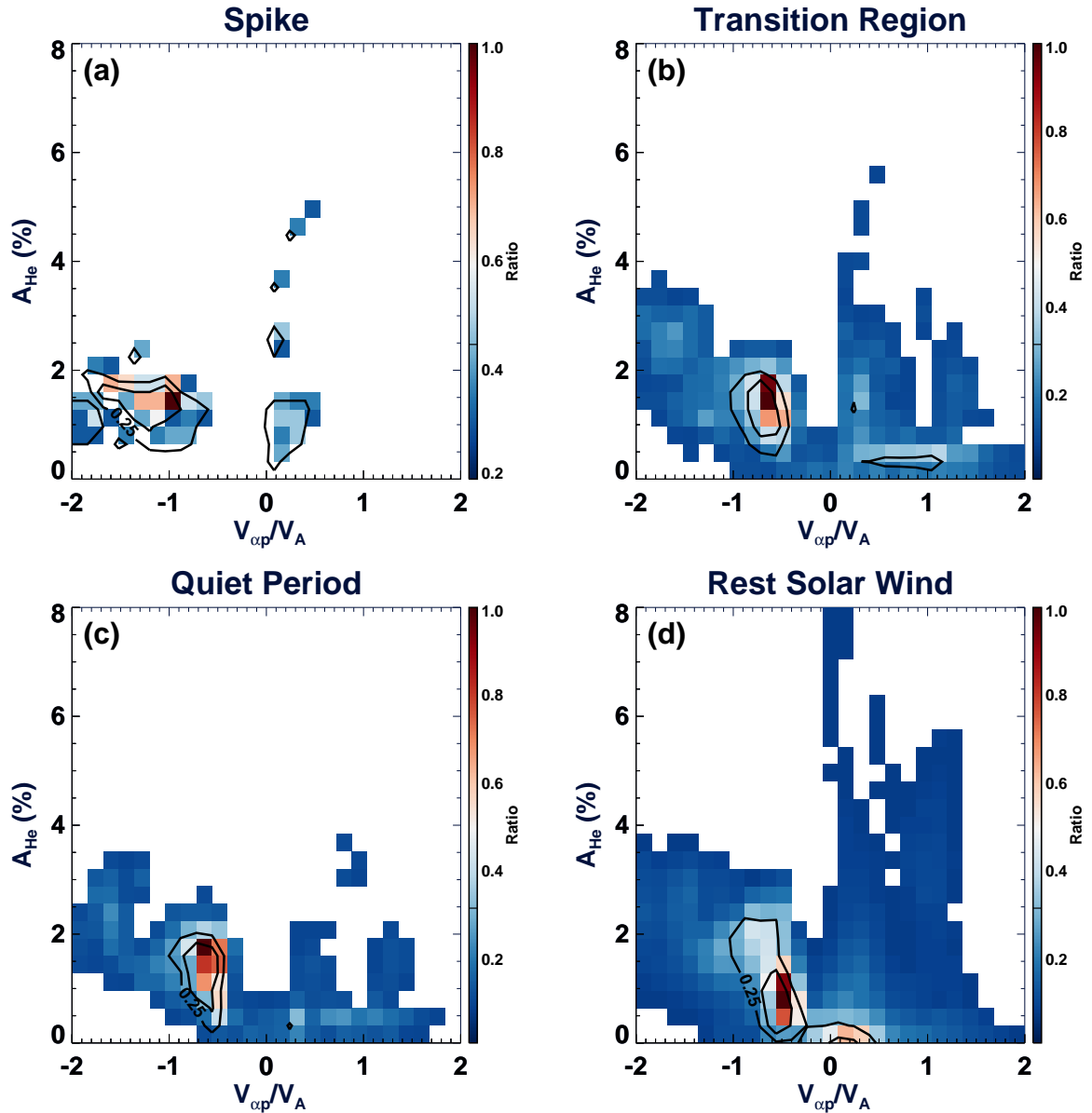


**Figure 5.** The distributions of alpha to proton abundance ratios ( $A_{\text{He}}$ ) versus the alpha-proton differential speed normalized by local Alfvén speed ( $V_{\alpha p}/V_A$ ) inside and outside switchbacks. Panels (a) to (d) show the distributions in spike, combined transition region, combined quiet period, and rest solar wind, respectively. The colors in each panel indicate the ratio of data counts. The black lines indicate 25% and 50% measurement contours.

and helium-rich ( $A_{\text{He}} \sim 6.0\%$ ) populations exist in different parts of switchbacks, suggesting the switchbacks may originate from both closed and open magnetic field regions in the Sun. This is also supported by previous studies that the switchbacks are found both in slow and fast solar winds (Horbury et al. 2018, 2020; de Wit et al. 2020; Bale et al. 2021, e.g.). In addition, the  $A_{\text{He}}$  distributions show no significant difference inside and outside switchbacks, and the similar plasma indicates the switchback is an intact structure that have no big difference in different regions, which is consistent with latest work by McManus et al. (2022). Moreover, the helium-poor population overwhelms the helium-rich population in switchbacks, implying that solar wind from closed magnetic field regions contributes more to these switchbacks. The reason could be that the switchbacks are identified mainly from slow and intermediate speed solar wind during these encounters, as we find the solar wind with speed larger than 600 km/s, 500 km/s and 400 km/s is 0.31%, 0.85% and 6.71% of the time, respectively. Furthermore, figure 4(b) displays the  $A_{\text{He}}$  variations in

the combined regions of switchbacks. The  $A_{\text{He}}$  features are similar and more uniform in the combined regions as the asymmetry in leading and trailing edges are averaged.

In Figure 5, panels (a) to (d) show the variations of  $A_{\text{He}}$  versus the field-aligned  $V_{\alpha\text{p}}/V_{\text{A}}$  in spike, TR, QP and rest solar wind, respectively. The black lines in the figure indicate the 25% and 50% measurement contours. In the spike, the major solar wind shows low  $A_{\text{He}}$  ( $< 2.0\%$ ), whereas the  $V_{\alpha\text{p}}/V_{\text{A}}$  varies from -2 to 1. As introduced above,  $V_{\alpha\text{p}}$  is comparable to  $V_{\text{A}}$  in fast wind but close to zero in slow wind. Mostafavi et al. (2022) find that  $V_{\alpha\text{p}}$  increases toward the Sun but the magnitude is mainly below  $V_{\text{A}}$ , and alpha particles usually move faster than protons near the Sun, based on PSP observations. However, the high  $V_{\alpha\text{p}}/V_{\text{A}}$  in the solar wind may associate with the very low local Alfvén speed when magnetic field lines change polarities, or it may infer the preferential acceleration of alpha particles (Isenberg & Hollweg 1983; Kasper et al. 2017). We note that there are negative values of  $V_{\alpha\text{p}}/V_{\text{A}}$ , which could be a result of waves that slow down alpha particles but accelerate the protons as the energy of alpha particles overtakes protons (Ďurovcová et al. 2017). Therefore, the low  $A_{\text{He}}$  and low  $V_{\alpha\text{p}}/V_{\text{A}}$  ( $|V_{\alpha\text{p}}/V_{\text{A}}| < 0.7$ ) implies some of the switchbacks are formed by magnetic reconnection process, whereas the low  $A_{\text{He}}$  and high  $V_{\alpha\text{p}}/V_{\text{A}}$  ( $< -0.7$ ) indicates the possible slow down of alpha particles. There is a small portion of solar wind with high  $A_{\text{He}}$  (about 6.0%) and slightly high  $V_{\alpha\text{p}}/V_{\text{A}}$  (about 0.8), suggesting the wave-turbulence driven mechanism may also contribute. The  $A_{\text{He}} - V_{\alpha\text{p}}/V_{\text{A}}$  distributions are similar in TR and QP. The dominant population shows low  $A_{\text{He}}$  ( $< 4.0\%$ ) and low  $V_{\alpha\text{p}}/V_{\text{A}}$  ( $|V_{\alpha\text{p}}/V_{\text{A}}| < 1.0$ ), but  $V_{\alpha\text{p}}/V_{\text{A}}$  varies in a large range from about -2 to 2. Additionally, the TR solar wind also have a population with high  $A_{\text{He}}$  ( $\sim 6.0\%$ ) but low  $V_{\alpha\text{p}}/V_{\text{A}}$  (close to zero), which may suggest compressions in the transition regions that work to decrease the differential speed (Ďurovcová et al. 2019). Krasnoselskikh et al. (2020) and Larosa et al. (2021) also confirm the existence of compressible switchbacks. Therefore, in TR and QP, the magnetic reconnection mechanism works overwhelmingly to wave-turbulence driven mechanism, but compressions and/or waves are rich in these regions to change the  $A_{\text{He}} - V_{\alpha\text{p}}/V_{\text{A}}$  distributions. In rest solar wind, both  $A_{\text{He}}$  and  $V_{\alpha\text{p}}/V_{\text{A}}$  range from low to high values with predominant low  $A_{\text{He}}$  and low  $V_{\alpha\text{p}}/V_{\text{A}}$  population, indicating the reconnection mechanism dominates but other mechanisms also play a role.

## 4. DISCUSSION

### 4.1. The stability of switchback structures

The switchbacks are much more abundant in the inner heliosphere than beyond. One reason could be that the PSP provides higher time resolution measurements, which helps figure out more, especially, short-duration switchbacks. Another possible explanation for this is that the switchbacks may not be able to survive, if they are formed from the Sun, for a long heliocentric distance. If so, the stability of switchback structures could be a key to understand the evolution of switchbacks.

According to the distributions of small scale current sheets in switchbacks, we could infer that these current sheets should contribute to stabilize the switchback structures. In general, the small scale current sheets are a measure of the braiding of the magnetic field within the switchbacks. The magnetic braiding was proposed to explain the coronal heating by Parker (1972, 1988, 1994), with the hypothesis that the random, complex motions of footpoints at the base of coronal loops due to the photospheric turbulence could twist and entangle the magnetic field, and the coronal heating happens as the braided magnetic fields inevitably relax to a force-free state (Schrijver et al. 1998; Wilmot-Smith 2015). The relaxation of the braided field via magnetic reconnection processes would eventually result in a complex array of current sheets (Longbottom et al. 1998; Pontin et al. 2011; Ng et al. 2012; Rappazzo & Parker 2013). Prior & Yeates (2016a,b) construct different types of braided magnetic field and investigate their evolutions in background field, their detailed studies suggest that the braided internal structures can inhibit large scale morphological changes. Therefore, the small scale current sheets in switchbacks should also help to stabilize the switchback structures.

Additionally, the S-shape curvature of switchbacks may also help achieve stability. The S-shape magnetic field could form two large scale current sheets in both sides of a spike. Thus, the Lorentz force in the transverse direction could drag the magnetic structure together, and may further result in a magnetic component in this direction that work to stabilize the current sheets, which are well studied in different environments (refer to the review papers Zelenyi et al. 2010; Artemyev & Zimovets 2012; Treumann & Baumjohann 2013, and references therein). Furthermore, the compressions in transition regions, as we suggested in section 3.3, could resist the magnetic tensions to prevent the S-shape curvature from relaxing.

As a conclusion, we suggest the small scale current sheets in switchbacks and the S-shape curvatures of switchbacks may work together to stabilize their structures, and enable them to propagate stably into PSP space.

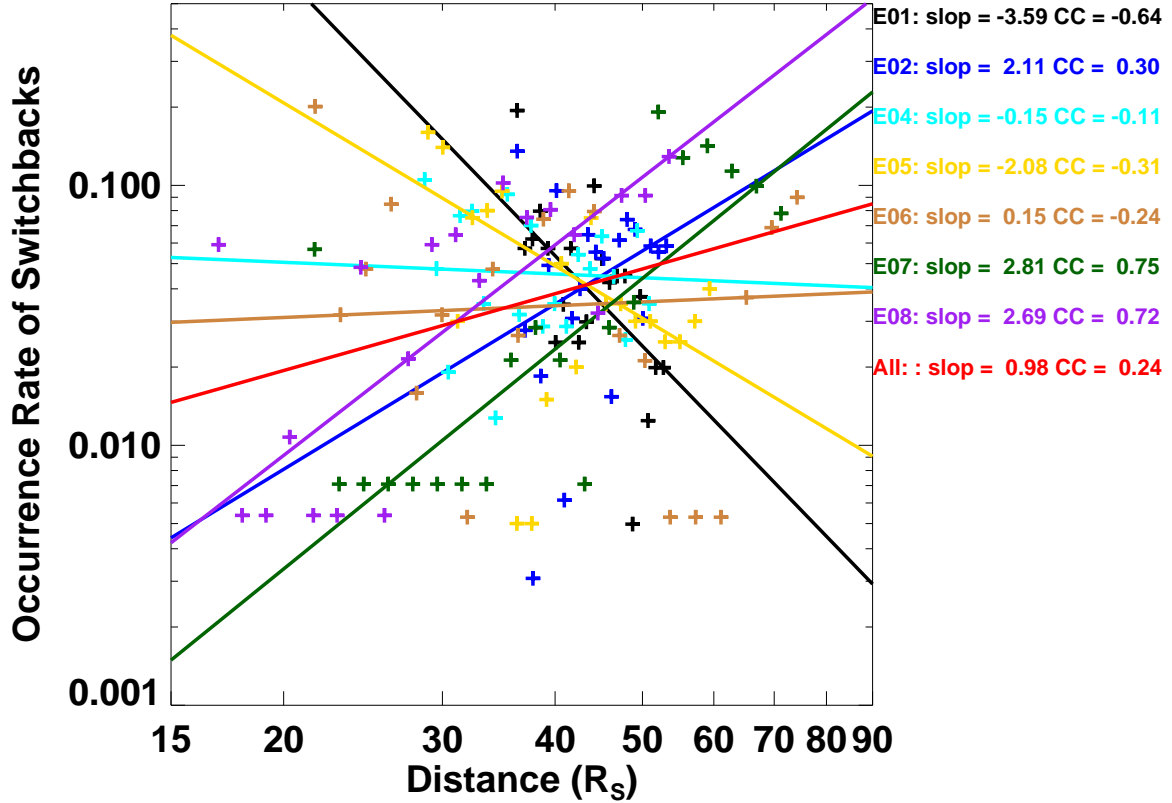


**Figure 6.** The occurrence rates of switchbacks during the seven encounters. The radial variations of occurrence rate of switchbacks are fitted with a linear function, and the fitted slope and correlation coefficient (CC) during each encounter are presented in the right figure with same color.

#### 4.2. The origins of switchbacks

The origins of switchbacks are still debatable. According to the introduction, current observations intend to support the solar origins of switchbacks through interchange reconnection processes near the Sun (Fisk & Kasper 2020; Drake et al. 2020; Woodham et al. 2020; Zank et al. 2020), but other formation methods can not be excluded.

The presence of small scale current sheets in switchbacks is consistent with the method that switchbacks are formed by interchange reconnection near the Sun. Interchange reconnection occurs between open magnetic flux and large coronal loops. Large coronal loops are stable structures, and the randomly braided field lines contribute to the stability of the original loops. Since the braiding is not easy to unwind, it is also not easy to unwind during the interchange reconnection process, and the resulting switchback has an inherent stability built in from its beginning. The small scale current sheets are more abundant inside switchbacks could be a reasonable consequence of the braided magnetic field. As the switchbacks propagate farther, the relaxation of braided magnetic field lines starts from the quiet region and spreads to the transition region and spike. Due to the relative long durations of transition regions, the spike may dissipate at last, but the relaxation of the braided field lines and the dissipation of current sheets will finally destroy some switchbacks. Consequently, we may further compare the switchback characteristics with this scenario. Mozer et al. (2020) find the Poynting flux increases significantly inside switchbacks. This is consistent with the magnetic braiding, which stores energy into the braided field (Ng et al. 2012; Yeates et al. 2014). Moreover, the braiding implies the flux tubes are tilted strongly with respect to each other (Borovsky 2008), which may lead to the large angular deflections of switchbacks (Horbury et al. 2020) and the Poynting flux enhancements with rotational angle (Mozer et al. 2020). Additionally, Larosa et al. (2021) show an interesting result on the distribution of discontinuities, they find that most switchbacks have a tangential discontinuity at the leading edge and a rotational discontinuity at the trailing edge, or vice versa. This special distribution may be in line with our scenario. In general, the complex topology of the braided field leads to the formation of tangential discontinuities (Parker 1972; Janse et al. 2010), while the interchange reconnection could generate rotational discontinuities (Lee et al. 1996; Lin et al. 2009). Thus, a



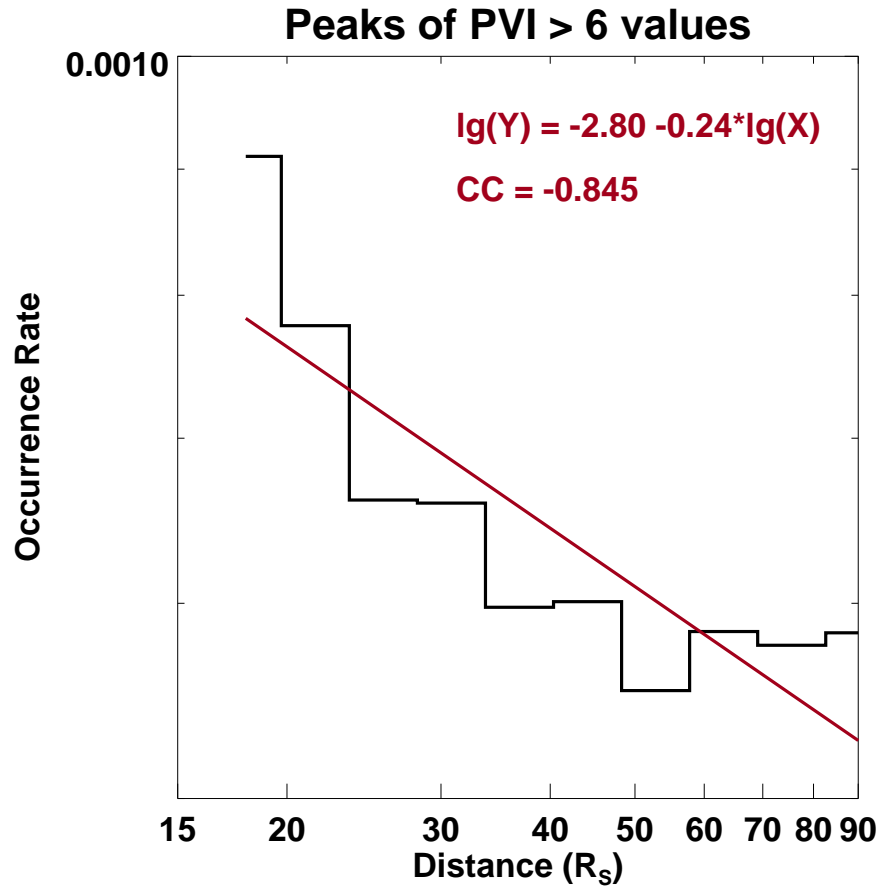


**Figure 7.** The occurrence rate of small scale current sheets as a function of distance from the Sun. The black histogram indicates the occurrence rate of current sheets at different distances, and the radial evolution is fitted by the red line, with the relationship presenting in the upper right of the figure.

switchback that forms from interchange reconnection should result in rotational discontinuity at the reconnection side whilst retain the tangential discontinuity at the other side. Besides, the "patch" distribution is a distinct signature of switchbacks (Horbury et al. 2020; Woolley et al. 2020). We may conceivably connect the "patch" switchbacks to the flux concentrations caused by the footpoint fragmentations at the edges of granules or supergranules (Schrijver et al. 1998; Berger & Asgari-Targhi 2009; Berger 2010), but we should carefully compare their time scales to check the consistency (Horbury et al. 2020; Bale et al. 2021; Fargette et al. 2022).

In addition, the fact that switchbacks occur in all types of solar winds further implies that they should come from all of their source regions in the corona (Fisk & Kasper 2020). The helium signatures of switchbacks also support these conclusions. We find both helium-rich and helium-poor populations inside and outside switchbacks, indicating their origins from both closed and open magnetic field regions in the Sun. The  $A_{\text{He}} - V_{\alpha\text{p}}/V_A$  distributions further suggest that the reconnection mechanism should dominate the formation processes, but the wave-turbulence driven mechanism should also contribute.

However, we could not exclude the possibility that the switchbacks may form in the interplanetary space. Macneil et al. (2020) give an evidence that the switchbacks observed by Helios increase with distances from 0.3 au to 1 au. They also note that the switchbacks are shorter than 40 s due to the data time resolution, and the occurrence rates at different distances are calculated with data samples, which may bring deviations due to solar wind expansions. Based on our database, 46.6% of the spikes are shorter than 40 s, thus these small switchbacks could significantly change the radial variations of switchbacks. In order to reduce the influences of solar wind expansions, which could be true as the durations of switchbacks seem to increase with heliocentric distances (not shown), we calculate the occurrence rates at different distances with the number of switchbacks at this distance to the total number of switchbacks in each encounter. As shown in figure 6, the occurrence rates of switchbacks during each encounter are presented with

different colored plus signs, and the according radial evolution relationships are displayed in right side. It denotes that the occurrence rates decrease with distance during E1 and E4-E5, but increase in E2 and E6-E8, implying that some switchbacks are probably formed in the interplanetary space. We note that the fitted relationships could change if we select different number of distance bins and the occurrence rates are somewhat scattering, we suppose this is related to the "patch" distributions of switchbacks (Horbury et al. 2020) and/or the different solar wind conditions in different encounters. If we use the data samples to calculate the occurrence rates, then we can see the rates also show increase and decrease trends in different encounters, suggesting the switchback durations indeed affect. In addition, the calculation of occurrence rates does not consider the solar wind conditions and the difference of the observation time at different distances. As PSP collects more data in the future orbits, we can then extend this analysis with less uncertainties.

Moreover, turbulence may also work to generate switchbacks, but it is not the primary formation mechanism based on our results. PVI values also measure the intermittency in the turbulence, thus large PVI values indicate strong intermittency in the turbulence. If the switchbacks are formed by turbulence, then we are expected to observe more switchbacks at places where large PVI values are more abundant. Figure 7 displays the occurrence rate of current sheets as a function of distance from the Sun, suggesting the current sheets decrease with the distance and approach to a steady state after about  $60 R_S$ . Consequently, if the above assumption is correct, we should see a decreasing trend of switchback occurrence with distance. However, figure 6 indicates the switchback occurrence rate can even increase with distance. Therefore, the contradiction implies that the turbulence could not be the primary formation mechanism of switchbacks.

#### 4.3. Other concerns

Focusing on the inverted magnetic field lines, current studies argue that they could be manifestations of appropriate crossings of magnetic field lines by spacecraft (Fisk & Kasper 2020; Macneil et al. 2020). On one hand, the switchback could be an intact structure that there is no abrupt changes of the solar stream during the crossing, i.e. the switchback is formed by the same flux tubes, which is supported by current observations (Mozer et al. 2020; Martinović et al. 2021; Woolley et al. 2020; McManus et al. 2022) and by our results that the  $A_{He}$  distributions are similar in different regions of switchbacks. On the other hand, the folded magnetic field lines could be formed by the propagation of ejecta or small transients (Drake et al. 2020; Macneil et al. 2020), thus the spacecraft may measure the structured solar wind at one side and the intact solar stream from the Sun at the other side. In this circumstance, the solar streams in the switchbacks, especially in LTR and TTR, could be very different, and thus bring bias to trace their origins and add asymmetry between leading and trailing edges. In future works, we may need to separate these switchbacks, and comparisons of the solar wind characteristics (such as the currents, proton entropy, distributions of suprathermal electrons, temperature anisotropies) in different regions of switchbacks are necessary to figure out whether a switchback is formed by the same bundle of flux tubes.

## 5. SUMMARY

In this work, we study the stability of switchback structures by investigating the distributions of small scale current sheets with PVI method. Our results show that the current sheets are more abundant in spike than both transition regions and quiet periods, and slight asymmetry seems to present in leading and trailing edges of switchbacks. Moreover, the occurrence rate of current sheets appears to decrease with radial distances from the Sun, suggesting they may work together with the S-shape magnetic field curvature of switchbacks to unite the switchback structures and enable them to propagate outward to be observed at least in PSP space.

The presence of small scale current sheets in the switchbacks also support the method that the switchbacks are formed through interchange reconnection processes, and some observational characteristics of switchbacks are consistent with this scenario. With the alpha measurements available in E4-E8, we analyze the  $A_{He}$  variations inside and outside switchbacks. It shows that helium-rich and helium-poor populations are observed in different regions of switchbacks, indicating the switchbacks come from both open and closed magnetic field regions in the Sun. Furthermore, the joint variations of  $A_{He}$  versus  $V_{\alpha p}/V_A$  further denote that low  $A_{He}$  and low  $V_{\alpha p}/V_A$  dominates in different regions of switchbacks, implying magnetic reconnection is the primary mechanism to produce the switchbacks. However, we can not exclude the possibility that some switchbacks may originate from the interplanetary space via other formation mechanisms.

## ACKNOWLEDGMENTS

Parker Solar Probe was designed, built, and is now operated by the Johns Hopkins Applied Physics Laboratory as part of NASA's Living with a Star (LWS) program (contract NNN06AA01C). Support from the LWS management and technical team has played a critical role in the success of the Parker Solar Probe mission. Thanks to the Solar Wind Electrons, Alphas, and Protons (SWEAP) team for providing data (PI: Justin Kasper, BWX Technologies). Thanks to the FIELDS team for providing data (PI: Stuart D. Bale, UC Berkeley). Jia Huang is also supported by NASA grant 80NSSC22K1017.

## REFERENCES

- Abbo, L., Ofman, L., Antiochos, S., et al. 2016, *Space Science Reviews*, 201, 55
- Aellig, M. R., Lazarus, A. J., & Steinberg, J. T. 2001, *Geophysical Research Letters*, 28, 2767
- Akhavan-Tafti, M., Kasper, J., Huang, J., & Bale, S. 2021, *Astronomy & Astrophysics*, 650, A4
- Akhavan-Tafti, M., Kasper, J., Huang, J., & Thomas, L. 2022, *The Astrophysical Journal Letters*, 937, L39
- Alterman, B., Kasper, J. C., Stevens, M. L., & Koval, A. 2018, *The Astrophysical Journal*, 864, 112
- Alterman, B. L., & Kasper, J. C. 2019, *The Astrophysical Journal Letters*, 879, L6
- Artemyev, A., & Zimovets, I. 2012, *Solar Physics*, 277, 283
- Bale, S., Goetz, K., Harvey, P., et al. 2016, *Space Science Reviews*, 204, 49
- Bale, S., Horbury, T., Velli, M., et al. 2021, *The Astrophysical Journal*, 923, 174
- Bale, S. D., Badman, S. T., Bonnell, J. W., et al. 2019, *Nature*, doi: [10.1038/s41586-019-1818-7](https://doi.org/10.1038/s41586-019-1818-7)
- Berger, L., Wimmer-Schweingruber, R., & Gloeckler, G. 2011, *Physical review letters*, 106, 151103
- Berger, M. A. 2010, in *Braids: Introductory Lectures on Braids, Configurations and Their Applications* (World Scientific), 305–328
- Berger, M. A., & Asgari-Targhi, M. 2009, *The Astrophysical Journal*, 705, 347
- Bochsler, P. 2007, *The Astronomy and Astrophysics Review*, 14, 1
- Borovsky, J. E. 2008, *Journal of Geophysical Research: Space Physics*, 113
- Borrini, G., Wilcox, J. M., Gosling, J. T., Bame, S. J., & Feldman, W. C. 1981, *J. Geophys. Res.*, 86, 4565, doi: [10.1029/JA086iA06p04565](https://doi.org/10.1029/JA086iA06p04565)
- Case, A. W., Kasper, J. C., Stevens, M. L., et al. 2020, *The Astrophysical Journal Supplement Series*, 246, 43
- Chen, C., Bale, S., Bonnell, J., et al. 2020, *The Astrophysical Journal Supplement Series*, 246, 53
- Chhiber, R., Goldstein, M. L., Maruca, B., et al. 2020, *The Astrophysical Journal Supplement Series*, 246, 31
- Crooker, N., Huang, C.-L., Lamassa, S., et al. 2004a, *Journal of Geophysical Research: Space Physics*, 109
- Crooker, N., Kahler, S., Larson, D., & Lin, R. 2004b, *Journal of Geophysical Research: Space Physics*, 109
- de Pablos, D., Samanta, T., Badman, S., et al. 2022, *Solar Physics*, 297, 1
- de Wit, T. D., Krasnoselskikh, V. V., Bale, S. D., et al. 2020, *The Astrophysical Journal Supplement Series*, 246, 39
- Drake, J. F., Agapitov, O., Swisdak, M., et al. 2020, Are switchbacks signatures of magnetic flux ropes generated by interchange reconnection in the corona? <https://arxiv.org/abs/2009.05645>
- Đurovcová, T., Němeček, Z., & Šafránková, J. 2019, *The Astrophysical Journal*, 873, 24
- Đurovcová, T., Šafránková, J., Němeček, Z., & Richardson, J. 2017, *The Astrophysical Journal*, 850, 164
- Fargette, N., Lavraud, B., Rouillard, A. P., et al. 2022, *A&A*, 663, A109, doi: [10.1051/0004-6361/202243537](https://doi.org/10.1051/0004-6361/202243537)
- . 2021, *The Astrophysical Journal*, 919, 96
- Farrell, W., MacDowall, R., Gruesbeck, J., Bale, S., & Kasper, J. 2020, *The Astrophysical Journal Supplement Series*, 249, 28
- Finley, A. J., McManus, M. D., Matt, S. P., et al. 2020, *Astronomy and Astrophysics*, doi: <https://doi.org/10.1051/0004-6361/202039288>
- Fisk, L. 2005, *The Astrophysical Journal*, 626, 563
- Fisk, L., & Kasper, J. 2020, *The Astrophysical Journal Letters*, 894, L4
- Fisk, L., & Schwadron, N. 2001, *The Astrophysical Journal*, 560, 425
- Fox, N. J., Velli, M. C., Bale, S. D., et al. 2016, *SSRv*, 204, 7, doi: [10.1007/s11214-015-0211-6](https://doi.org/10.1007/s11214-015-0211-6)
- Fu, H., Madjarska, M. S., Li, B., Xia, L., & Huang, Z. 2018, *Monthly Notices of the Royal Astronomical Society*, 478, 1884

- Gosling, J. T., Asbridge, J. R., Bame, S. J., et al. 1981, *J. Geophys. Res.*, 86, 5438, doi: [10.1029/JA086iA07p05438](https://doi.org/10.1029/JA086iA07p05438)
- Greco, A., Chuychai, P., Matthaeus, W., Servidio, S., & Dmitruk, P. 2008, *Geophysical Research Letters*, 35
- Greco, A., Matthaeus, W., Perri, S., et al. 2018, *Space Science Reviews*, 214, 1
- He, J., Zhu, X., Yang, L., et al. 2020, Possible Generation Mechanism for Compressional Alfvénic Spikes as Observed by Parker Solar Probe. <https://arxiv.org/abs/2009.09254>
- Horbury, T., Matteini, L., & Stansby, D. 2018, *Monthly Notices of the Royal Astronomical Society*, 478, 1980
- Horbury, T. S., Woolley, T., Laker, R., et al. 2020, *The Astrophysical Journal Supplement Series*, 246, 45
- Huang, J., Liu, Y. C.-M., Klecker, B., & Chen, Y. 2016a, *Journal of Geophysical Research: Space Physics*, 121, 19
- Huang, J., Liu, Y. C.-M., Qi, Z., et al. 2016b, *Journal of Geophysical Research: Space Physics*, 121
- Huang, J., Liu, Y. C.-M., Peng, J., et al. 2017, *Journal of Geophysical Research (Space Physics)*, 122, 6927, doi: [10.1002/2017JA023906](https://doi.org/10.1002/2017JA023906)
- Huang, J., Liu, Y. C.-M., Peng, J., et al. 2018, *Journal of Geophysical Research: Space Physics*, 123, 7167
- Isenberg, P. A., & Hollweg, J. V. 1983, *Journal of Geophysical Research: Space Physics*, 88, 3923
- Janse, Å., Low, B., & Parker, E. 2010, *Physics of Plasmas*, 17, 092901
- Kahler, S., Crocker, N., & Gosling, J. 1996, *Journal of Geophysical Research: Space Physics*, 101, 24373
- Kasper, J., Stevens, M., Korreck, K., et al. 2012, *The Astrophysical Journal*, 745, 162
- Kasper, J., Klein, K., Lichko, E., et al. 2021, *Physical review letters*, 127, 255101
- Kasper, J. C., Stevens, M. L., Lazarus, A. J., Steinberg, J. T., & Ogilvie, K. W. 2007, *The Astrophysical Journal*, 660, 901
- Kasper, J. C., Abiad, R., Austin, G., et al. 2016, *Space Science Reviews*, 204, 131
- Kasper, J. C., Klein, K. G., Weber, T., et al. 2017, *The Astrophysical Journal*, 849, 126
- Kasper, J. C., Bale, S. D., Belcher, J. W., et al. 2019, *Nature*, doi: [10.1038/s41586-019-1813-z](https://doi.org/10.1038/s41586-019-1813-z)
- Krasnoselskikh, V., Larosa, A., Agapitov, O., et al. 2020, *The Astrophysical Journal*, 893, 93
- Larosa, A., Krasnoselskikh, V., de Wit, T. D., et al. 2021, *Astronomy and Astrophysics-A&A*, 650, A3
- Lavraud, B., Fargette, N., Réville, V., et al. 2020, *The Astrophysical journal letters*, 894, L19
- Lee, L., Lin, Y., & Choe, G. 1996, *Solar Physics*, 163, 335
- Liang, H., Zank, G., Nakanotani, M., & Zhao, L.-L. 2021, *The Astrophysical Journal*, 917, 110
- Lin, C.-C., Tsai, C.-L., Chen, H., et al. 2009, *Journal of Geophysical Research: Space Physics*, 114
- Liu, M., Issautier, K., Meyer-Vernet, N., et al. 2021, arXiv preprint arXiv:2101.03121
- Livi, R., Larson, D. E., Kasper, J. C., et al. 2022, *The Astrophysical Journal*, 938, 138, doi: [10.3847/1538-4357/ac93f5](https://doi.org/10.3847/1538-4357/ac93f5)
- Longbottom, A., Rickard, G., Craig, I. J., & Sneyd, A. D. 1998, *The Astrophysical Journal*, 500, 471
- Macneil, A. R., Owens, M. J., Wicks, R. T., et al. 2020, *Monthly Notices of the Royal Astronomical Society*, 494, 3642
- Mallet, A., Squire, J., Chandran, B. D., Bowen, T., & Bale, S. D. 2021, *The Astrophysical Journal*, 918, 62
- Marsch, E., Mühlhäuser, K.-H., Rosenbauer, H., Schwenn, R., & Neubauer, F. 1982, *Journal of Geophysical Research: Space Physics*, 87, 35
- Martinović, M. M., Klein, K. G., Huang, J., et al. 2021, *The Astrophysical Journal*, 912, 28
- McComas, D., Hoogeveen, G., Gosling, J., et al. 1996, *Astronomy and Astrophysics*, 316, 368
- McManus, M. D., Bowen, T. A., Mallet, A., et al. 2020, *The Astrophysical Journal Supplement Series*, 246, 67
- McManus, M. D., Verniero, J., Bale, S. D., et al. 2022, *The Astrophysical Journal*, 933, 43
- Moncuquet, M., Meyer-Vernet, N., Issautier, K., et al. 2020, *The Astrophysical Journal Supplement Series*, 246, 44
- Mostafavi, P., Allen, R., McManus, M., et al. 2022, *The Astrophysical Journal Letters*, 926, L38
- Mozer, F. S., Agapitov, O. V., Bale, S. D., et al. 2020, *The Astrophysical Journal Supplement Series*, 246, 68, doi: [10.3847/1538-4365/ab7196](https://doi.org/10.3847/1538-4365/ab7196)
- Ng, C., Lin, L., & Bhattacharjee, A. 2012, *The Astrophysical Journal*, 747, 109
- Nisticò, G., Bothmer, V., Patsourakos, S., & Zimbardo, G. 2010, *AnGeo*, 28, 687
- Parker, E. 1972, *The Astrophysical Journal*, 174, 499
- Parker, E. N. 1988, *The Astrophysical Journal*, 330, 474
- . 1994, *Spontaneous current sheets in magnetic fields: with applications to stellar x-rays* (Oxford University Press)
- Podesta, J. J. 2017, *Journal of Geophysical Research: Space Physics*, 122, 2795
- Pontin, D., Wilmot-Smith, A., Hornig, G., & Galsgaard, K. 2011, *Astronomy & Astrophysics*, 525, A57
- Prior, C., & Yeates, A. 2016a, *Astronomy and Astrophysics*, 587, A125
- . 2016b, *Astronomy and Astrophysics*, 591, A16

- Pulupa, M., Bale, S., Bonnell, J., et al. 2017, *Journal of Geophysical Research: Space Physics*, 122, 2836
- Qudsi, R., Maruca, B., Matthaeus, W., et al. 2020, *The Astrophysical Journal Supplement Series*, 246, 46
- Rappazzo, A., & Parker, E. 2013, *The Astrophysical Journal Letters*, 773, L2
- Rasca, A. P., Farrell, W. M., MacDowall, R. J., Bale, S. D., & Kasper, J. C. 2021, *The Astrophysical Journal*, 916, 84
- Reisenfeld, D. B., Gary, S., Gosling, J., et al. 2001, *Journal of Geophysical Research: Space Physics*, 106, 5693
- Schrijver, C., Title, A., Harvey, K., et al. 1998, *Nature*, 394, 152
- Schwadron, N., & McComas, D. 2021, *The Astrophysical Journal*, 909, 95
- Shi, C., Panasenco, O., Velli, M., et al. 2022, *The Astrophysical Journal*, 934, 152
- Shoda, M., Chandran, B. D., & Cranmer, S. R. 2021, *The Astrophysical Journal*, 915, 52
- Squire, J., Chandran, B. D., & Meyrand, R. 2020, *The Astrophysical Journal Letters*, 891, L2
- Steinberg, J., Lazarus, A., Ogilvie, K., Lepping, R., & Byrnes, J. 1996, *Geophysical research letters*, 23, 1183
- Sterling, A. C., & Moore, R. L. 2020, arXiv preprint arXiv:2006.04990
- Suess, S., Ko, Y.-K., Von Steiger, R., & Moore, R. 2009, *Journal of Geophysical Research: Space Physics*, 114
- Szabo, A., Larson, D., Whittlesey, P., et al. 2020, *The Astrophysical Journal Supplement Series*, 246, 47
- Telloni, D., Zank, G. P., Stangalini, M., et al. 2022, *The Astrophysical Journal Letters*, 936, L25, doi: [10.3847/2041-8213/ac8104](https://doi.org/10.3847/2041-8213/ac8104)
- Tenerani, A., Velli, M., Matteini, L., et al. 2020, *The Astrophysical Journal Supplement Series*, 246, 32
- Tian, H., McIntosh, S. W., Wang, T., et al. 2012, *The Astrophysical Journal*, 759, 144
- Tomczyk, S., McIntosh, S., Keil, S., et al. 2007, *Science*, 317, 1192
- Treumann, R. A., & Baumjohann, W. 2013, *Frontiers in Physics*, 1, 31
- Verniero, J., Larson, D., Livi, R., et al. 2020, *The Astrophysical Journal Supplement Series*, 248, 5
- Whittlesey, P. L., Larson, D. E., Kasper, J. C., et al. 2020, *The Astrophysical Journal Supplement Series*, 246, 74
- Wilmot-Smith, A. 2015, *Philosophical Transactions of the Royal Society A: Mathematical, Physical and Engineering Sciences*, 373, 20140265
- Woodham, L., Horbury, T., Matteini, L., et al. 2020, arXiv preprint arXiv:2010.10379
- Woolley, T., Matteini, L., Horbury, T. S., et al. 2020, arXiv preprint arXiv:2007.10906
- Yamauchi, Y., Suess, S. T., Steinberg, J. T., & Sakurai, T. 2004, *Journal of Geophysical Research: Space Physics*, 109
- Yeates, A., Bianchi, F., Welsch, B., & Bushby, P. 2014, *Astronomy & Astrophysics*, 564, A131
- Zank, G., Nakanotani, M., Zhao, L.-L., Adhikari, L., & Kasper, J. 2020, *The Astrophysical Journal*, 903, 1
- Zelenyi, L. M., Petrukovich, A., Artemyev, A. V., Malova, K. V., & Nakamura, R. 2010, *Physics-Usppekhi*, 53, 933